Oriented Event Shapes for massive Quarks

Alejandro Bris[1,2,*], *Néstor G.* Gracia[3,**], and *Vicent* Mateu[3,***]

[1]Departamento de Física Teórica, Universidad Autónoma de Madrid, E-28049, Madrid, Spain
[2]Instituto de Física Teórica UAM-CSIC, E-28049 Madrid, Spain
[3]Departamento de Física Fundamental e IUFFyM, Universidad de Salamanca, E-37008 Salamanca, Spain

Abstract. In this work we present the computation of so-called oriented event-shape distributions for massive quarks up to $O(\alpha_s)$, along with the total oriented cross section in which one does not look at the geometric properties of the momentum distribution for particles in the final state. We consider the vector and axial-vector currents, and for the former, we find a non-vanishing result at $O(\alpha_s^0)$ that translates into a significant enhancement as compared to the massless approximation. Our results are an important ingredient for analyses that aim to determine the strong coupling with high accuracy.

1 Introduction

State-of-the art predictions for event shapes with massive quarks are less advanced than those for massless particles. Similarly, our theoretical knowledge of oriented event shapes is significantly worse than that of observables in which the orientation of the event is ignored. We aim to reduce these two gaps by computing the NLO fixed-order expressions of massive-quark-initiated oriented event shapes, for differential, cumulative and total cross sections.

We consider the process $e^+e^- \to$ hadrons initiated by a $Q\overline{Q}$ pair, with Q a massive quark, and define the event orientation by the angle θ_T between the thrust axis and the beam direction. The thrust axis $\hat{n}$ is the unit vector appearing in the definition of thrust [1]:

$$\tau = 1 - \max_{\hat{n}} \frac{\sum_i |\vec{p}_i \cdot \hat{n}|}{\sum_i |\vec{p}_i|}\,, \tag{1}$$

that maximizes the sum. It can be shown that it is always parallel to the sum of the 3-momenta of a subset of final-state particles within the same hemisphere. In Ref. [2] it was shown that to fully determine the orientation of the cross section it is enough to specify two θ_T-independent structures:

$$\frac{1}{\sigma_0}\frac{\mathrm{d}\sigma}{\mathrm{dcos}(\theta_T)\mathrm{d}e} = \frac{3}{8}[1+\cos^2(\theta_T)]\frac{1}{\sigma_0}\frac{\mathrm{d}\sigma}{\mathrm{d}e} + [1-3\cos^2(\theta_T)]\frac{1}{\sigma_0}\frac{\mathrm{d}\sigma_{\mathrm{ang}}}{\mathrm{d}e}\,, \tag{2}$$

*e-mail: alejandro.bris@uam.es
**e-mail: ngonzalez@usal.es
***e-mail: vmateu@usal.es

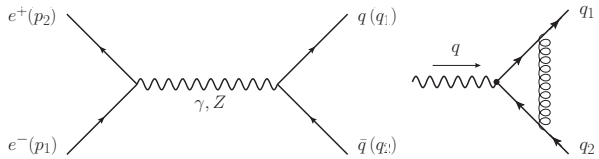

Figure 1: Feynman diagrams for the partonic process $e^+e^- \to Q\overline{Q}$ at LO and NLO.

with e a generic event shape and σ_0 the Born cross section. The first term is the unoriented distribution, while the second, dubbed the angular term, is the one we focus on. In the rest of this write-up we denote the minimal value that the event shape e can take by $e_{\min}$. It does not depend on the number of partons in the final state, and it is attained in the physical situation in which the quark and the anti-quark are produced in conjunction with any number of massless particles with zero energy. Therefore the soft singularities will take place for $e \to e_{\min}$, that is, for dijet configurations.

In our computations we use dimensional regularization to deal with both ultraviolet (UV) and infrared (IR) divergences. For the latter one has to work out the 2- and 3-particle phase space in $d = 4 - 2\varepsilon$ dimensions, differential in the polar angles of the quarks. To that end we used the Gram-Schmidt procedure to consistently construct a suitable set of axes in our vector space with a non-integer number of dimensions. When combining real- and virtual-radiation contributions we end up with a finite result.

2 Lowest order Result

We start off with the $O(\alpha_s^0)$ results, which are computed in $d = 4-2\varepsilon$ dimensions even though they are UV and IR finite. This is still very useful as one can normalize the cross sections with the d-dimensional point-like cross section to have nice-looking intermediate results. The relevant Feynman diagram is shown in the left panel of Fig. 1. At this point it is instructive to introduce the total angular cross section:

$$R_{\text{ang}} = \int \mathrm{d}e \frac{1}{\sigma_0}\frac{\mathrm{d}\sigma_{\text{ang}}}{\mathrm{d}e} \equiv \sum_{n=0}^{\infty}\left[\frac{\alpha_s(\mu)}{\pi}\right]^n R_n^{\text{ang},C}\,, \tag{3}$$

which does not depend on the specific choice for e. Using the d-dimensional 2-particle phase space differential in the polar angle

$$\frac{1}{2s}\frac{\mathrm{d}Q_2}{\mathrm{dcos}(\theta)} = \frac{\beta^{1-2\varepsilon}\sin^{-2\varepsilon}(\theta)}{2^{5-4\varepsilon}s^{1+\varepsilon}\Gamma(1-\varepsilon)\pi^{1-\varepsilon}}\,, \tag{4}$$

with $s = Q^2$ the center-of-mass energy squared, and where we have already included the flux factor, a relatively simple computation yields[1]

$$\sigma_B = N_c Q_q^2 \frac{(4\pi)^{1+\varepsilon}(1-\varepsilon)\Gamma(2-\varepsilon)\alpha_{\text{em}}^2}{(3-2\varepsilon)\Gamma(2-2\varepsilon)s^{1+\varepsilon}}, \qquad R_0^{\text{ang},V} = \frac{3\hat{m}^2\beta}{4}\,, \qquad R_0^{\text{ang},A} = 0\,, \tag{5}$$

where we have set $\varepsilon = 0$ in $R_0^{\text{ang},C}$ but kept an arbitrary d in the point-like cross section. Here $\beta \equiv \sqrt{1-4\hat{m}^2}$ is the quark velocity and $\hat{m} = m/Q$ its reduced mass. The non-vanishing

[1] All results are presented in the pole mass scheme.

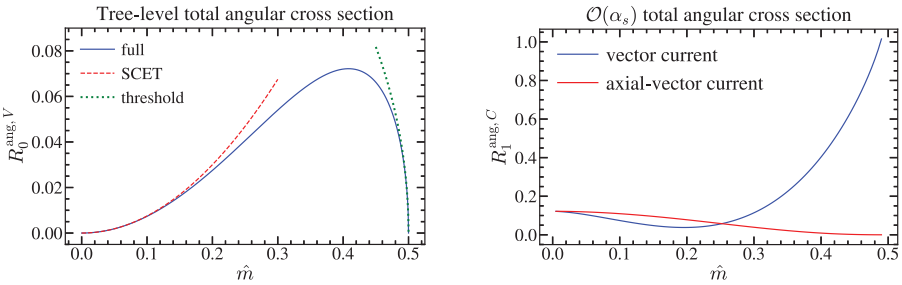

Figure 2: Total angular cross section at LO for the vector current (left panel) and NLO (right panel) for vector (blue) and axial-vector (red) currents.

result for $R_0^{\mathrm{ang},V}$ implies an enhancement with respect to the massless approximation and the appearance of IR divergences at NLO, which translate into singular distributional structures in differential cross sections. These results can be converted into differential distributions simply multiplying by $\delta(e - e_{\min})$. The LO result for $R_0^{\mathrm{ang},V}$ is shown graphically in the left panel of Fig. 2, together with its SCET and threshold approximations.

3 Virtual radiation

The relevant diagram for this contribution appears in the right panel of Fig. 2. To carry out this computation we use the known result for the massive quark form factors for vector and axial-vector currents

$$V^\mu = \left[1 + C_F \frac{\alpha_s}{\pi} A(\hat{m})\right]\gamma^\mu + C_F \frac{\alpha_s}{\pi} \frac{B(\hat{m})}{2m}(q_1 - q_2)^\mu \,, \tag{6}$$
$$A^\mu = \left[1 + C_F \frac{\alpha_s}{\pi} C(\hat{m})\right]\gamma^\mu\gamma_5 + C_F \frac{\alpha_s}{\pi} \frac{D(\hat{m})}{2m}\gamma_5\, q^\mu \,,$$

with $q = q_1 + q_2$ and $q_{1,2}$ the photon, quark and anti-quark momenta, respectively. Only the terms A, B and C contribute due to vector current conservation on either the quark or lepton sides, and we only need the real part of them [3, 4]

$$\mathrm{Re}[A(\hat{m})] = \left(\frac{1+\beta^2}{2\beta}\log\left(\frac{1+\beta}{2\hat{m}}\right) - \frac{1}{2}\right)\left[\frac{1}{\varepsilon} - 2\log\left(\frac{m}{\mu}\right)\right] + A_{\mathrm{reg}}(\hat{m}) \,, \tag{7}$$
$$A_{\mathrm{reg}}(\hat{m}) = \frac{3}{2}\beta\log\left(\frac{1+\beta}{2\hat{m}}\right) - 1 + \frac{1+\beta^2}{4\beta}\left[\pi^2 - 2\log^2\left[\frac{1+\beta}{2\hat{m}}\right] - 2\,\mathrm{Li}_2\left(\frac{2\beta}{1+\beta}\right)\right],$$
$$\mathrm{Re}[C(\hat{m})] = \mathrm{Re}[A(\hat{m})] + \frac{4\hat{m}^2}{\beta}\log\left(\frac{1+\beta}{2\hat{m}}\right).$$

Keeping an arbitrary d in both currents, after adding the flux factor and integrating the d-dimensional 2-body phase space we find

$$R_{21}^{\mathrm{ang},V} = \frac{\beta}{2}\left\{\left[1 - \frac{2}{\beta}(1-2\hat{m}^2)\log\left(\frac{1+\beta}{2\hat{m}}\right)\right]\left[2\hat{m}^2\log\left(\frac{m}{\mu}\right) - \frac{\hat{m}^2}{\varepsilon} + \frac{3}{10}(3-2\hat{m}^2) + 2\hat{m}^2\log(\beta)\right]\right.$$
$$\left. + 2\hat{m}^2\mathrm{Re}[A_{\mathrm{reg}}(\hat{m})] - \hat{m}^2\beta\log\left(\frac{1+\beta}{2\hat{m}}\right)\right\},$$
$$R_{21}^{\mathrm{ang},A} = \frac{9\beta^2}{5}\left[\frac{\beta}{2} - (1-2\hat{m}^2)\log\left(\frac{1+\beta}{2\hat{m}}\right)\right], \tag{8}$$

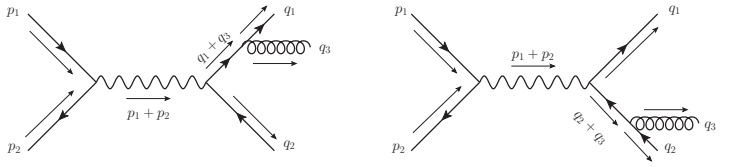

Figure 3: Diagrams for NLO real-radiation contributions.

where the $1/\varepsilon$ singularity in the vector current is of IR origin. To convert these two results into differential distributions one simply multiplies them by $\delta(e - e_{\min})$. The fact that our results do not vanish in the massless limit is an artifact of dimensional regularization. When added to the real-radiation contribution all artifacts and divergences cancel.

4 Real radiation

Before discussing the real-radiation computation, we show the general form of the differential distribution for massive quarks up to NLO:

$$\frac{1}{\sigma_0^C}\frac{\mathrm{d}\sigma_{\mathrm{ang}}^C}{\mathrm{d}e} = R_{\mathrm{ang}}^{0,C}(\hat{m})\,\delta[e - e_{\min}(\hat{m})] + C_F\frac{\alpha_s(\mu)}{\pi}A_e^{\mathrm{ang},C}(\hat{m})\delta[e - e_{\min}(\hat{m})] \\ + C_F\frac{\alpha_s(\mu)}{\pi}B_{\mathrm{plus}}^{\mathrm{ang},C}(\hat{m})\left[\frac{1}{e - e_{\min}(\hat{m})}\right]_+ + C_F\frac{\alpha_s(\mu)}{\pi}F_{C,e}^{\mathrm{ang}}(e,\hat{m}) + O(\alpha_s^2)\,, \tag{9}$$

where $F_{C,e}^{\mathrm{ang}}$ is an integrable function in the vicinity of $e = e_{\min}$ and the rest of structures are distributions globally referred to as 'singular terms'. It is easy to see that $F_{C,e}^{\mathrm{ang}}$ and $B_{\mathrm{plus}}^{\mathrm{ang},C}$ come only from diagrams with more than two particles in the final state while $A_e^{\mathrm{ang},C}$ has contributions from both virtual and real radiation. Finally, for the axial-vector current, all terms except for $F_{A,e}^{\mathrm{ang}}$ are zero.

The modulus squared of the sum of amplitudes shown in Fig. 3, sumed over final polarizations and averaged over initial ones, can be written as

$$\overline{\sum_\lambda}|M|^2 = \frac{8\pi^2 C_F}{s}\left(\frac{\mu^2 e^{\gamma_E}}{4\pi}\right)^{\varepsilon}[A_0^C + A_1^C\beta_1^2\cos^2(\theta_1) + A_2^C\beta_2^2\cos^2(\theta_2) + A_{12}^C\beta_1\beta_2\cos(\theta_1)\cos(\theta_1)]\,, \tag{10}$$

where $\theta_{1,2}$ are the angles between the beam and the quark/anti-quark 3-momentum. The analytic form of the A_i^C coefficients will be given elsewhere. To translate this result into a cross section we need the d-dimensional 3-particle phase space, differential in the polar angles of the quark and the anti-quark:

$$\frac{\mathrm{d}Q_3}{2s} = \frac{4^\varepsilon s^{-2\varepsilon}}{2(4\pi)^{4-2\varepsilon}\Gamma(1-2\varepsilon)}\int \mathrm{d}x_1\mathrm{d}x_2\mathrm{d}\cos(\theta_i)\mathrm{d}\cos(\theta_j)\frac{\beta_i^{-2\varepsilon}\beta_j^{-2\varepsilon}\theta(h_{ij})}{h_{ij}^{1/2+\varepsilon}}\,, \tag{11}$$

$$h_{ij} = \sin^2(\tilde{\theta}_{ij}) - \cos^2(\theta_i) - \cos^2(\theta_j) + 2\cos(\tilde{\theta}_{ij})\cos(\theta_i)\cos(\theta_j) \\ \equiv [\cos(\theta_i) - \cos(\theta_{ij}^-)][\cos(\theta_{ij}^+) - \cos(\theta_i)]\,,$$

$$\cos(\theta_{ij}^\pm) = \cos(\tilde{\theta}_{ij})\cos(\theta_j) \pm \sin(\tilde{\theta}_{ij})\sin(\theta_j) = \cos(\tilde{\theta}_{ij} \mp \theta_j)\,.$$

where $x_i = 2E_i/Q$ are dimensionless variables proportional to the energy of each particle. We use $i = 1, 2$ and 3 to label the quark, antiquark and gluon, respectively. We have defined

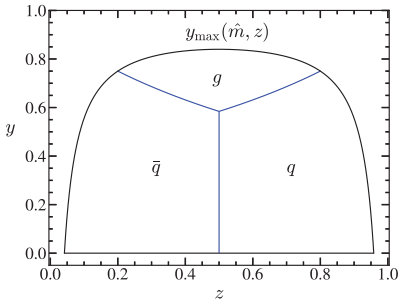

Figure 4: Phase space for three particles (two quarks with equal mass plus a massless gluon) in (z, y) coordinates.

$\beta_i \equiv 2|\vec{p}_i|/Q = \sqrt{x_i^2 - 4\hat{m}_i^2}$. The results above serve to compute the multi-differential cross section at NLO:

$$\frac{1}{\sigma_0^C}\frac{\mathrm{d}^4\sigma^C_{\alpha_s}}{\mathrm{d}x_1\mathrm{d}x_2\mathrm{dcos}(\theta_i)\mathrm{dcos}(\theta_j)} = \frac{4^\varepsilon\alpha_s C_F}{16\pi^2}\frac{(3-2\varepsilon)(1-2\varepsilon)}{(1-\varepsilon)\Gamma(2-\varepsilon)}\left(\frac{\mu^2 e^{\gamma_E}}{s}\right)^\varepsilon \frac{\beta_i^{-2\varepsilon}\beta_j^{-2\varepsilon}}{h_{ij}^{1/2+\varepsilon}} \times[A_0^C + A_1^C\beta_1^2\cos^2(\theta_1) + A_2^C\beta_2^2\cos^2(\theta_2) + A_{12}^C\beta_1\beta_2\cos(\theta_1)\cos(\theta_1)], \tag{12}$$

From the expression above we can project out the angular distribution differential in the quark and anti-quark energy in d dimensions:

$$\frac{1}{\sigma_0^C}\frac{\mathrm{d}^2\sigma^{\alpha_s,C}_{\mathrm{ang}}}{\mathrm{d}z\mathrm{d}y} = \frac{3\alpha_s C_F}{8\pi}\frac{y^{1-2\varepsilon}}{(1-\varepsilon)^2\Gamma(1-\varepsilon)}\left(\frac{\mu^2 e^{\gamma_E}}{s}\right)^\varepsilon [(1-y)(1-z)z - \hat{m}^2]^{-\varepsilon} \times\left\{A_q^C(\hat{m},y,z)\theta\left(z-\frac{1}{2}\right)\theta[y_\tau(\hat{m},1-z)-y] + A_{\bar{q}}^C(\hat{m},y,z)\theta\left(\frac{1}{2}-z\right)\theta[y_\tau(\hat{m},z)-y] + A_g^C(\hat{m},y,z)\theta[y-y_\tau(\hat{m},z)]\theta[y-y_\tau(\hat{m},1-z)]\right\}, \tag{13}$$

where we used the symmetric kinematic variables (y, z) defined through the change of variables $x_1 = 1-(1-z)y$, $x_2 = 1-zy$, such that the soft limit has been mapped to $y \to 0$. The form of the phase space in these variables is shown in Fig. 4. The functions $A^C_{q,\bar{q},g}$ depend linearly on the A_i^C defined in Eq. (10) with coefficients that depend on $y, z, \hat{m}$ and ε. The exact relation will be given elsewhere, but we provide the result after working out the combination for the axial current setting $\varepsilon = 0$ — since there are no IR singularities — [we do not show results for $A^C_{\bar{q}}$ since by symmetry arguments one can show that $A^C_{\bar{q}}(\hat{m},y,z) = A^C_q(\hat{m},y,1-z)$]

$$A_q^A(\hat{m},y,z) = \frac{(1-y)z^2 - \hat{m}^2 z\{2-y^2+z[2+y(y-2)]\} + 2\hat{m}^4}{z^2\{[1-y(1-z)]^2 - 4\hat{m}^2\}}, \qquad A_g^A(\hat{m},y,z) = \frac{2(1-y)(1-z)^2z^2 - \hat{m}^2(1-z)z(4-y^2-2y) + 2\hat{m}^4}{y^2(1-z)^2z^2}. \tag{14}$$

For the vector current, keeping only the linear dependence in ε where it is strictly necessary we find

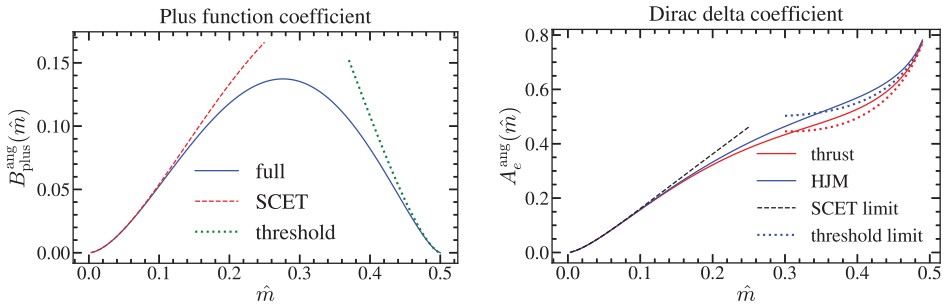

Figure 5: Coefficients of the singular structures for the vector-current differential distribution, as appearing in Eq. (16).

$$A_q^V(\hat m,y,z)=\frac{V^{\rm div}(\hat m,z)+V^{\varepsilon}(\hat m,z)\varepsilon}{y^2}+V^{\rm fin}(y,z,\hat m)\,, \tag{15}$$

$$V^{\rm fin}(\hat m,y,z)=\frac{(1-y)y(1-z)z^2-\hat m^2 z[2-y(1-2z^2)]+2\hat m^4[y(1-z)+4z]}{y(1-z)z^2\{[1-y(1-z)]^2-4\hat m^2\}}\,.$$

$$V^{\rm div}(\hat m,z)=-2\hat m^2 M_V^1(\hat m,z)\,,\qquad V^{\varepsilon}(\hat m,z)=\frac{9+14\hat m^2}{5}M_V^1(\hat m,z)\,,$$

$$A_g^V(\hat m,y,z)=\frac{2[(1-y)z(1-z)-\hat m^2]}{y^2(1-z)z}\,,\qquad M_V^1(\hat m,z)=-\frac{(1-z)z-\hat m^2}{(1-z)^2z^2}\,.$$

In terms of those we find the following analytic results for the vector-current coefficients multiplying the singular structures:

$$A_e^{\rm ang}(\hat m)=\frac{3}{4}[A_\delta(\hat m)-2\hat m^2 I_e(\hat m)]\,,\qquad B^{\rm ang}_{\rm plus}(\hat m)=\frac{3\hat m^2}{2}\left[2(1-2\hat m^2)\log\left(\frac{1+\beta}{2\hat m}\right)-\beta\right], \tag{16}$$

$$A_\delta(\hat m)=\hat m^2\Big\{2\beta[\log(\hat m)-1]+\frac{1+\beta^2}{2}\Big[\pi^2-2L_\beta^2+{\rm Li}_2\Big(\frac{2\beta}{\beta-1}\Big)-3\,{\rm Li}_2\Big(\frac{2\beta}{\beta+1}\Big)$$
$$-4\log\Big(\frac{1+\beta}{2\hat m}\Big)[\log(\hat m)-1]\Big]\Big\},$$

$$I_e(\hat m)=-\int_{z_-}^{\frac12}{\rm d}z M_V^1(\hat m,z)\log[f_e(z)]\,,$$

where $I_e(\hat m)$ has been analytically computed in Ref. [5] for a large set of event shapes. We present graphically the form of $A_e^{\rm ang}(\hat m)$ for a couple of event shapes in Fig. 5, along with the universal $B^{\rm ang}_{\rm plus}$ coefficient.

5 Numerical Analysis

Integrating the differential distribution of Eq. (13) in the full d-dimensional phase space and adding the virtual-diagram contribution one obtains the NLO total angular cross section. Explicit analytic results shall be presented elsewhere, but a graphical representation is shown in the right panel of Fig. 2. The computation of the differential and cumulative distributions for $e > e_{\rm min}$ can be organized such that only $d = 4$ expressions become necessary. For the mass-sensitive event shapes 2-jettiness [6] (closely related to thrust) and heavy jet mass [7–9] we have found analytic expressions for the differential distributions, while we have been able to

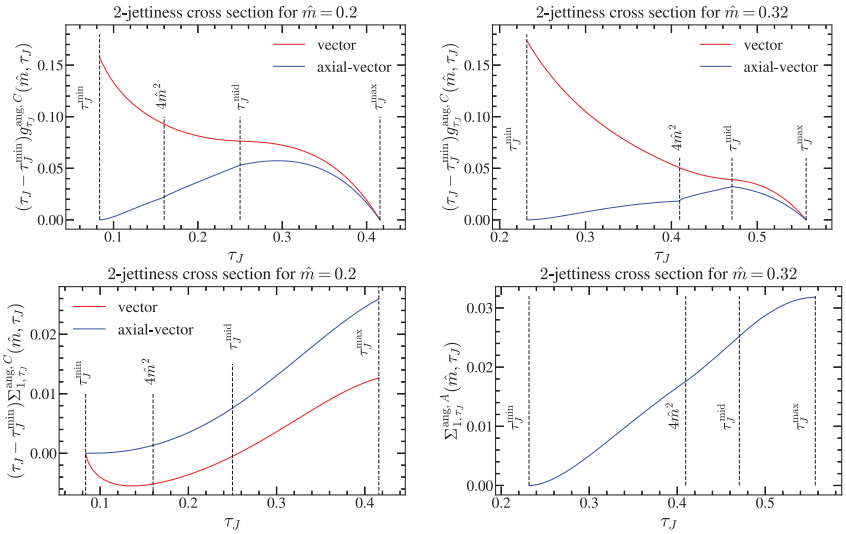

Figure 6: Differential and cumulative cross sections for thrust and heavy jet mass for values of the reduced mass below and above m_{crit}.

write down their cumulative counterparts in terms of 1-dimensional numerical integrals. We do not show explicit expressions here, but present results in a numerical form in Fig. 6, where both vector and axial-vector currents are represented for two values of the reduced mass $\hat{m}$. We mark with vertical dashed lines the points of the spectrum where kinks or discontinuities can happen. For the moment it suffices to say that both the minimal and maximal values of those two event shapes, $e_{\min}$ and $e_{\max}$, depend on the reduced mass and become equal for $\hat{m} = 1/2$. The discussion on how these points appear and their analytic expressions shall be presented elsewhere. It is worth commenting on the result for heavy jet mass, since its behavior is different depending on the value of $\hat{m}$. There is a critical value $\hat{m}_{\text{crit}} \approx 0.286169$ above which there is a region with zero cross section within the physical spectrum. The cumulative cross section is totally flat in this patch. This behavior is of kinematic origin and therefore takes place for both currents. There is no such effect for 2-jettiness.

Finally, we present an analysis of the impact of the bottom quark mass as a correction to the massless prediction for the total oriented cross section R_{ang}, see Fig. 7. This observable is of high relevance since it is a prominent candidate to determine the strong coupling fitting to experimental data. This is so because, due to inclusive nature, it suffers from small hadronization effects and Sudakov-log resummation might not be necessary, but at the same time, at lowest order it is already linearly dependent on α_s. In our analysis, first we assume one can experimentally tag on bottom quarks (for example through the presence of B mesons in the final state) and on the current (for instance counting the number of pions), and second, consider a more realistic scenario in which no tagging is applied. In this latter situation we find that the massive correction at NLO for $Q = 20, 50$ and $100\,\text{GeV}$ is as large as 38%, 4.27% and 1.11%, respectively. Therefore it cannot be neglected in any analysis that aims for high precision.

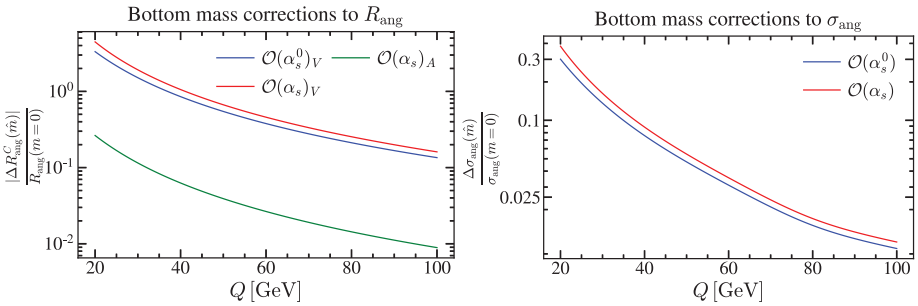

Figure 7: Bottom mass corrections to the total angular cross section.

6 Conclusions

We have presented fixed-order results for oriented event shapes at NLO considering massive quarks. The computation has been organized such that the relevant angular distribution is projected out at a very early stage, and chosen a d-dimensional normalization that avoids having unphysical logs at intermediate steps. Bottom mass corrections turn out to be a very large correction to the massless approximation for LEP and smaller energies. An immediate application for our computation is the determination of the strong couplings by a comparison to existing experimental data on $R_{\rm ang}$. Our results for the total oriented cross section reveal a Sommerfeld enhancement at threshold, such that this observable might be useful to determine the top quark mass at a future e^+e^- collider through threshold scans.

References

[1] E. Farhi, Phys. Rev. Lett. **39**, 1587 (1977)
[2] V. Mateu, G. Rodrigo, JHEP **1311**, 030 (2013), 1307.3513
[3] J. Jersak, E. Laermann, P.M. Zerwas, Phys. Rev. **D25**, 1218 (1982), [Erratum: Phys. Rev.D36,310(1987)]
[4] B.W. Harris, J.F. Owens, Phys. Rev. **D65**, 094032 (2002), hep-ph/0102128
[5] C. Lepenik, V. Mateu, JHEP **03**, 024 (2020), 1912.08211
[6] I.W. Stewart, F.J. Tackmann, W.J. Waalewijn, Phys.Rev. **D81**, 094035 (2010), 0910.0467
[7] L. Clavelli, Phys.Lett. **B85**, 111 (1979)
[8] T. Chandramohan, L. Clavelli, Nucl.Phys. **B184**, 365 (1981)
[9] L. Clavelli, D. Wyler, Phys.Lett. **B103**, 383 (1981)